Nanoscale

PAPER

View Article Online
View Journal | View Issue

Cite this: *Nanoscale*, 2015, **7**, 16890

Lactoferrin conjugated iron oxide nanoparticles for targeting brain glioma cells in magnetic particle imaging

Asahi Tomitaka, Hamed Arami, Sonu Gandhi and Kannan M. Krishnan*

Received 30th April 2015,
Accepted 13th September 2015

DOI: 10.1039/c5nr02831k

www.rsc.org/nanoscale

Magnetic Particle Imaging (MPI) is a new real-time imaging modality, which promises high tracer mass sensitivity and spatial resolution directly generated from iron oxide nanoparticles. In this study, monodisperse iron oxide nanoparticles with median core diameters ranging from 14 to 26 nm were synthesized and their surface was conjugated with lactoferrin to convert them into brain glioma targeting agents. The conjugation was confirmed with the increase of the hydrodynamic diameters, change of zeta potential, and Bradford assay. Magnetic particle spectrometry (MPS), performed to evaluate the MPI performance of these nanoparticles, showed no change in signal after lactoferrin conjugation to nanoparticles for all core diameters, suggesting that the MPI signal is dominated by Néel relaxation and thus independent of hydrodynamic size difference or presence of coating molecules before and after conjugations. For this range of core sizes (14–26 nm), both MPS signal intensity and spatial resolution improved with increasing core diameter of nanoparticles. The lactoferrin conjugated iron oxide nanoparticles (Lf-IONPs) showed specific cellular internalization into C6 cells with a 5-fold increase in MPS signal compared to IONPs without lactoferrin, both after 24 h incubation. These results suggest that Lf-IONPs can be used as tracers for targeted brain glioma imaging using MPI.

Introduction

Magnetic nanoparticles, if suitably optimized and made biocompatible have translational potential in a variety of biomedical applications ranging from imaging to therapy.[1] Due to their small size and large surface-to-volume ratio, nanoparticles are particularly effective as carriers for drug delivery, provided they are properly functionalized. They also have advantages such as increased efficiency for targeted chemotherapy and reduced side effects.[2] Specifically, because of their magnetic properties and biocompatibility, superparamagnetic iron oxide nanoparticles have been used for various biomedical applications, such as drug and gene delivery,[3–5] magnetic resonance imaging (MRI) contrast agents,[3,6] biosensors,[7] magnetic cell separation,[8] hyperthermia treatment,[9,10] and magnetic particle imaging (MPI).[11–13] MPI is a new real-time imaging modality[11] that can be potentially used for performing quantitative, 3D *in vivo* imaging of magnetic nanoparticles with high tracer mass sensitivity and spatial resolutions.[12–14] While other established whole body imaging modalities such as computed tomography (CT) and MRI provide comparable spatial resolution, CT requires iodine contrast agents that have a high risk of contrast-induced nephropathy (CIN), particularly to patients with chronic kidney disease (CKD).[15] MPI promises greater sensitivity compared to MRI as its signal is directly generated from magnetic nanoparticles with magnetization more than 10^7 times of the weak proton signal exploited in MRI. Furthermore, the tissues surrounding nanoparticles are diamagnetic and provide negligible background in MPI images, resulting in near-infinite contrasts and improving imaging specificity for molecular imaging applications.[15] This combination of high sensitivity, no background signal interference, high contrast and a safe, biocompatible tracer, makes MPI a potentially strong candidate for molecular/targeted imaging applications. Recent reports also show that synergistic application of MPI with other whole-body imaging modalities such as MRI and near infra-red fluorescent (NIRF) imaging can be used for high sensitivity targeting and high resolution anatomical imaging.[16,17]

MPI exploits the nonlinear magnetization response of superparamagnetic iron oxide nanoparticles to an applied alternating magnetic field.[18] During measurements nanoparticles are excited by an alternating magnetic field and the time-varying magnetization response induces an inductive signal in the pick-up coils. Signal localization of the received

Materials Science & Engineering Department, University of Washington, Seattle, WA 98195-2120, USA. E-mail: kannanmk@uw.edu; Fax: +206-543-3100; Tel: +206-543-2814

signal is achieved by an additional field gradient (selection field), which provides either a single field-free point (FFP) or field-free line (FFL) that is then scanned over the entire imaging volume. At any time, the magnetization of nanoparticles outside of FFP or FFL is saturated, thus no signal is induced. Only the nanoparticles within the FFP or FFL respond to the alternating magnetic field and induce a spatially-sensitive signal for image reconstruction.[11]

For potential clinical applications, MPI signal optimization is crucial to achieve high spatial resolutions and signal-to-noise ratios (SNR). Since the MPI signal is controlled by dynamic magnetization reversal of the nanoparticle tracers, it is important to tune the relaxation mechanism of nanoparticles by controlling their physical parameters such as core and hydrodynamic diameter, magnetization, and anisotropy. The MPI performance with various particle core and hydrodynamic diameters, size distributions, and under different environments has been studied previously.[13,19–21] The nanoparticles investigated in those studies were coated with polymers that were designed for vascular imaging applications, optimized for maximum blood circulation and lacked targeting capability. However, for molecular imaging applications, it is necessary to functionalize nanoparticles with specific targeting ligands while ensuring that their optimized magnetic relaxation characteristics are not compromised. To achieve this functionalization, we first introduced carboxyl groups on the surface of nanoparticles using poly(maleic anhydride-*alt*-1-octadecene), which enables conjugation of various targeting ligands. Then, we conjugated lactoferrin as a ligand for brain tumor targeting.

Lactoferrin is a multifunctional glycoprotein, which belongs to the transferrin family, and possesses various biological functions such as antimicrobial, antibacterial, antiviral, antiparasitic, and antitumor activities.[22] Furthermore, low-density lipoprotein receptor-related protein (LRP), a specific lactoferrin receptor with excellent selectivity, is highly expressed in glioma cells.[23,24] Lactoferrin is also able to cross the blood–brain–barrier (BBB) through the transcytosis processes within brain capillary endothelial cells.[25] Because of their ability to target glioma cells and cross the blood–brain–barrier (BBB), lactoferrin-conjugated nanoparticles have great potential for brain tumor targeting.[25,26] Previous studies also have shown that lactoferrin-conjugated nanoparticles have no effect on cell viability.[23]

In this paper, lactoferrin was conjugated to monodisperse iron oxide nanoparticles optimized as MPI tracers. We investigated the physical and magnetic properties of the nanoparticles before and after lactoferrin conjugation, the influence of lactoferrin conjugation on MPI performance and internalization into glioma cells. The capability of lactoferrin conjugated iron oxide nanoparticles (Lf-IONPs) as MPI tracer was assessed using *in vitro* magnetic particle spectrometry (MPS). These results show that our monodisperse Lf-IONPs optimized for MPI can be used for brain tumor imaging, and this high sensitivity imaging has the potential to allow early diagnosis of brain tumors.

Experimental

Materials

Iron(III) chloride, anhydrous (98%) was purchased from Alfa-Aesar. Oleic acid (technical grade, 90%), 1-octadecene (technical grade, 90%), chloroform (HPLC, ≥99.8%), methanol (HPLC, ≥99.9%), poly(maleic anhydride-*alt*-1-octadecene) (M_n 30 000–50 000), *N*-(3-dimethylaminopropyl)-*N*′-ethylcarbodiimide hydrochloride (commercial grade, powder), *N*-hydroxysulfosuccinimide sodium salt (≥98%, HPLC), lactoferrin from human milk (≥85%, SDS-PAGE, lyophilized powder), paraformaldehyde powder (95%), potassium hexa-cyanoferrate(II) trihydrate, DAPI, alminum sulfate hydrate (98%), Dulbecco's phosphate buffered saline, and dimethyl sulphoxide (DMSO) Hybri-Max™ were purchased from Sigma-Aldrich. Sodium hydroxide solution 1 N, hydrochloric acid 1 N solution, and sodium bicarbonate were purchased from Fisher Scientific. Dulbecco's modified Eagle medium (DMEM) and 0.25% trypsin-EDTA were purchased from Gibco. Coomassie protein assay reagent was purchased from Thermo Scientific. All the reagents were used without further purification. Amicon® Ultra centrifugal filters ultracel®-50 K was purchased from Merck Millipore. Cy5.5™ Mono NHS Ester was purchased from GE Health Care.

Synthesis of iron oxide nanoparticles

Iron oleate precursors were synthesized following previously published methods.[27,28] Iron oxide nanoparticles were synthesized by the pyrolysis of the iron oleate precursor with excess oleic acid surfactant in 1-octadecene.[10] Synthesized nanoparticles were purified with a mixture of chloroform and methanol three times by magnetic decantation. Purified nanoparticles were dried in vacuum for more than 30 min.

Phase transfer

250 mg of poly(maleic anhydride-*alt*-1-octadecene) (PMAO) was dissolved in 2.5 ml of chloroform, and 5 mg of iron oxide nanoparticles were dispersed into 2.5 ml of chloroform by sonication. PMAO solution was added to iron oxide nanoparticles and sonicated for 2 h. Then, excess amount of 0.1 M sodium hydroxide solution was added and sonicated for 1 h. Chloroform was evaporated using rotary evaporator at 35 °C, 100 rpm for 90 min. Iron oxide nanoparticles transferred to sodium hydroxide solution were concentrated using centrifugal filter with the cut-off molecular weight of 50 K. The solution was purified with deionized (DI) water by three times centrifugation at 14 100*g* for 1 h. In order to improve the targeting uniformity and enhance the MPI signal intensity and resolution, aggregated nanoparticles were removed by centrifugation at 3000*g* for 15 min, and supernatant was collected. The final nanoparticle solution was neutralized using PD-10 column balanced with DI water.

Lactoferrin conjugation

250 μl of 10 mg ml^{-1} *N*-(3-dimethylaminopropyl)-*N*′-ethylcarbodiimide hydrochloride (EDC), 250 μl of 10 mg ml^{-1} *N*-hydroxy-

sulfosuccinimide sodium salt, and 7 μl of 1 M sodium hydroxide solution were mixed. 0.5 mg of iron oxide nanoparticles were added and sonicated for 15 min to activate the carboxyl group on the surface. Excess EDC and sulfo-NHS were removed using PD-10 column balanced with 10 mM phosphate buffered-saline solution (PBS, pH 7.4). 250 μl of 1 mg ml^{-1} lactoferrin was added to the activated iron oxide nanoparticles, and reacted overnight at room temperature. To purify the nanoparticles, they were centrifuged (12 000*g*, 1 h), and re-dispersed in PBS for three times. The supernatant was collected for detecting the concentration of lactoferrin by Bradford assay. Resulting nanoparticles were centrifuged at 1000–3000*g* for 15 min and the supernatant was collected to remove aggregates.

Characterization of iron oxide nanoparticles

The morphology of iron oxide and lactoferrin conjugated iron oxide nanoparticles were characterized by Transmission Electron Microscope (TEM, FEI Tecnai™ G2 F20), equipped with a Gatan CCD camera operated at 200 KeV. The magnetization curves were measured using a vibrating sample magnetometer (VSM, Lakeshore) at room temperature. Saturation magnetization was determined by assuming density equal to stoichiometric magnetite (5180 kg m^{-3}). The hydrodynamic diameters and zeta potentials of PMAO coated iron oxide nanoparticles (PMAO-IONPs) and lactoferrin conjugated iron oxide nanoparticles (Lf-IONPs) were measured by Zetasizer Nano-ZS (Malvern instruments, Worcestershire, UK). 20 μl of PMAO-IONPs and Lf-IONPs were dispersed in DI water and 10 mM phosphate buffered-saline solution (PBS, pH 7.4), respectively. Water was used for PMAO-IONPs due to their lack of long term stability in PBS. Iron concentration was determined using Inductively Couple Plasma Atomic Emission Spectrophotometer (ICP-AES, Jarrell Ash, US).

The lactoferrin concentration conjugated on the surface of the iron oxide nanoparticles was determined by Bradford assay. The concentration of the protein within the supernatant was measured, and the amount of lactoferrin on the nanoparticles was obtained by deducting the amount of lactoferrin in the supernatant from that added in the reaction. The experiments were performed in quadruplicate.

The binding affinity of lactoferrin conjugated to the surface of iron oxide nanoparticles was determined by the AssayMax Human Lactoferrin ELISA Kit (Assaypro) according to the manufacturer's protocols. A standard curve was prepared with free lactoferrin to compare the binding affinity of lactoferrin conjugated on iron oxide nanoparticles and free lactoferrin. The experiments were performed in quadruplicate.

Magnetic particle imaging

MPI performance was measured using a custom-built magnetic particle spectrometer (MPS) with the excitation field of 17 mT μ_0^{-1} at 26.0 kHz. The MPS excites magnetization of iron oxide nanoparticles using a transmit coil, and the time-varying magnetization (dm/dt) of nanoparticles induces a voltage signal in a receiver coil that will be used to generate the field-dependent differential susceptibility, (dm/dH), proportional to the MPI signal.[20,29] As we have shown before, MPS can be used as a quick measurement to verify the magnetic relaxation regime of the nanoparticles, and its results match well with other conventional techniques such as ac susceptometry and magnetorelaxometry.[30] 200 μl of nanoparticle solutions at concentrations of 0.190–0.958 mg Fe ml^{-1} were transferred to 0.6 ml microcentrifuge tubes and inserted into the system coil. Measurement was performed in triplicate. MPS data was analyzed using procedures published previously.[29] The obtained signal was normalized by the amount of iron in each sample, which was measured using ICP-AES. AC hysteresis loops were calculated from the same data by integration of the MPS signal or the measured differential susceptibility.

Cell culture

C6 glioma cells were cultured in Dulbecco's modified Eagle medium (DMEM, GIBCO Life Technologies Co., Carlsbad, CA, USA) supplemented with 10 vol% bovine fetal calf serum (FCS, Hyclone Laboratories, Inc., Utah, USA) at 37 °C in humidified atmosphere of 5% CO_2. The cells were trypsinized with 0.25% trypsin-EDTA, and re-suspended in DMEM medium for further experiments.

Cellular internalization

Prussian blue staining was performed to investigate the localization of lactoferrin iron oxide nanoparticles in C6 cells. Cells were seeded at 1×10^5 cells per well in 96-well plates (CELLSTAR, Greiner Bio-One, Monroe, US) and incubated for 24 h at 37 °C. The medium was exchanged with 50 μl of fresh medium containing 200 μg ml^{-1} of Lf-IONPs, and incubated for 24 h. After incubation, the cells were washed with PBS three times, and fixed in 4% paraformaldehyde at room temperature. Then, the solution containing 5% Potassium hexa-cyanoferrate(II) trihydrate and 10 vol% hydrochloric acid was added to each well (100 μl per well). The cells were incubated at room temperature for 30 min, and rinsed with PBS. Image analysis was performed using VWR inverted microscope and cells were viewed through a high-aperture 20× objective lens. Images were acquired using a V5MP 5.0 MP USB 2.0 digital camera with the software Motic Images Plus 2.0 ML.

Confocal microscopy was used to investigate the internalization of lactoferrin conjugated iron oxide nanoparticles in C6 cells. For this study, 0.01 ml of 10 mg ml^{-1} Cy5.5-NHS dissolved in DMSO was added into 0.1 ml of 10 mg ml^{-1} lactoferrin dissolved in sodium bicarbonate (0.1 M, pH 8.3). This mixture was incubated for 4 h at room temperature, and purified by using centrifugal filter with the cut-off molecular weight of 50 K. Conjugation of Cy5.5 labelled lactoferrin conjugated iron oxide nanoparticles was conducted with the same method as described in lactoferrin conjugation. Cells were seeded at 1×10^5 cells per well in Chamber Slide (Lab Tek II chamber slide system, Nalge Nunc International, Naperville, US) and incubated for 24 h at 37 °C. The medium was exchanged by 75 μl of fresh medium containing 200 μg ml^{-1} of Cy5.5 labelled Lf-IONPs. After incubation for 24 h, the cells

were washed with PBS three times, fixed in 4% PFA at room temperature for 30 min, stained with DAPI for 30 min at room temperature, and mounted with mounting medium (VECTASHIELD HardSet Mounting Medium, Vector Laboratories, Burlingame, US), and stored at 4 °C overnight. Cells were viewed through a Zeiss LSM 710 confocal microscope equipped with a high-aperture 63× objective lens. Images were taken with the ZEN software and analyzed with Image J.

In vitro MPI (magnetic particle imaging)

MPI performance of lactoferrin conjugated iron oxide nanoparticles internalized into C6 cells was measured using a custom-built magnetic particle spectrometer (MPS). Cells were seeded at 1×10^5 cells per well in 24 well plates (CELLSTAR, Greiner Bio-One, Monroe, US) and incubated for 24 h at 37 °C. The medium was exchanged by 200 μl of fresh medium containing 200 μg ml^{-1} of PMAO-IONPs or Lf-IONPs, and incubated for different time (4, 12, 24 h). The cells were washed with PBS three times, and trypsinized with 0.25% Trypsin-EDTA. After centrifuge, the cell pellet was dissolved in 150 μl of PBS, transferred to 0.6 ml microcentrifuge tubes, and then inserted into the MPS system. MPI performance was measured with the excitation field of 17 mT μ_0^{-1} at 26.0 kHz. Measurement was performed in triplicate. MPS data was analyzed using procedures published previously.[29] To measure the amount of Lf-IONPs internalized into C6 cells, the cells were lysed with concentrated hydrochloric acid. After an appropriate dilution of lysate with DI water, the amount of iron was measured by Inductively Couple Plasma Atomic Emission Spectrophotometer (ICP-AES, Jarrell Ash 955, US).

Results and discussion

Our previous results show that synthesis of iron oxide nanoparticles with narrow core size distribution is crucial for enhanced MPI performance.[13,20] Monodisperse iron oxide nanoparticles with core diameters of 14–26 nm were synthesized by thermal decomposition of iron oleate. These hydrophobic iron oxide nanoparticles were transferred to water using PMAO through hydrophobic interaction between the oleic acid and octadecene aliphatic chains of the PMAO.[31] The maleic anhydride groups of PMAO were hydrolysed in sodium hydroxide solution, and carboxyl groups were introduced on the surface of the nanoparticles for further functionalization with lactoferrin. These carboxyl groups were activated using EDC/NHS, and lactoferrin was covalently attached to the activated nanoparticles (Fig. 1).

The conjugation of lactoferrin was evaluated by measuring the hydrodynamic diameter and zeta potential of the nanoparticles, and using Bradford assay. Physical characteristics of PMAO coated iron oxide nanoparticles (PMAO-IONPs) and lactoferrin conjugated iron oxide nanoparticles (Lf-IONPs) with core diameters of 14 nm (14 nm-Lf-IONPs), 16 nm (16 nm-Lf-IONPs), 20 nm (20 nm-Lf-IONPs), 24 nm (24 nm-Lf-IONPs), and 26 nm (26 nm-Lf-IONPs) are shown in Table 1. The core diameters and their standard deviations were determined from TEM images, assuming a log-normal size distribution. The hydrodynamic diameters of PMAO-IONPs were 46–52 nm. Hydrodynamic diameter of the nanoparticles increased by 22–25 nm from the core diameter after conjugation of lactoferrin. Considering the size of lactoferrin molecules, ideally, we expect ~8 nm increase in hydrodynamic size of the nanoparticles after lactoferrin conjugation. However, the final hydrodynamic sizes of the lactoferrin coated nanoparticles were slightly larger than these ideal sizes. This was due to presence of negligible traces of crosslinked nanoparticles in the samples. Zeta potential of the nanoparticles also changed after lactoferrin conjugation. The zeta potential of PMAO-IONPs dispersed in DI water was between −35 to −43 mV, which indicates the existence of deprotonated carboxyl groups on the surface of PMAO-IONPs.[31] In contrast, Lf-IONPs dispersed in PBS, which is a commonly used biological medium, showed slightly negative zeta potential between −4 mV to −11 mV. The increase in hydrodynamic diameter and zeta potential of the nanoparticles confirmed the effective conjugation of lactoferrin to the surface of nanoparticles. Also, previous gel electrophoresis and Fourier transform infrared spectroscopy (FTIR) studies showed successful conjugation of lactoferrin to nanoparticles using EDC/NHS reactions.[23] In addition, we used Bradford assay to quantify the number of lactoferrin molecules conjugated to the nanoparticles (Table 2). As we show in Fig. 4B, our nanoparticles had a fluorescent signal generated from Cy5.5-labelled lactoferrin molecules, which further supports presence of lactoferrin on nanoparticles.

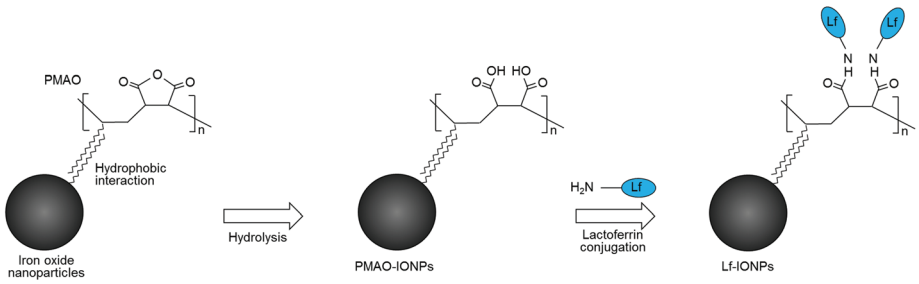

Fig. 1 Schematic representation of phase transfer using PMAO and lactoferrin conjugation to iron oxide nanoparticles.

Table 1 Characterization data of PMAO coated iron oxide nanoparticles (PMAO-IONPs) and lactoferrin conjugated iron oxide nanoparticles (Lf-IONPs)

Sample name	Core diameter	Magnetization Ms	Hydrodynamic diameter	Zeta potential
14 nm-PMAO-IONPs	14 nm, $\sigma = 0.15$	311 kA m^{-1}	49 nm	−43 mV
14 nm-Lf-IONPs		306 kA m^{-1}	74 nm	−7 mV
16 nm-PMAO-IONPs	16 nm, $\sigma = 0.10$	306 kA m^{-1}	48 nm	−43 mV
16 nm-Lf-IONPs		306 kA m^{-1}	70 nm	−8 mV
20 nm-PMAO-IONPs	20 nm, $\sigma = 0.14$	337 kA m^{-1}	52 nm	−41 mV
20 nm-Lf-IONPs		326 kA m^{-1}	75 nm	−6 mV
24 nm-PMAO-IONPs	24 nm, $\sigma = 0.10$	342 kA m^{-1}	50 nm	−41 mV
24 nm-Lf-IONPs		322 kA m^{-1}	72 nm	−11 mV
26 nm-PMAO-IONPs	26 nm, $\sigma = 0.16$	322 kA m^{-1}	46 nm	−35 mV
26 nm-Lf-IONPs		342 kA m^{-1}	71 nm	−4 mV

Table 2 The amount of lactoferrin conjugated to iron oxide nanoparticles and number of lactoferrin per iron oxide nanoparticle measured by Bradford assay

Sample name	Lactoferrin [μg per mg Fe_3O_4]	Lactoferrin/particle	% of lactoferrin conjugated
14 nm-Lf-IONPs	447	22	89%
17 nm-Lf-IONPs	471	35	94%
20 nm-Lf-IONPs	475	69	95%
24 nm-Lf-IONPs	401	101	80%
26 nm-Lf-IONPs	434	138	87%

The nanoparticles showed expected superparamagnetic and magnetization behaviours with variation consistent with their core sizes after PMAO coating or lactoferrin conjugation.

Bradford assay was conducted to quantify the amount of lactoferrin conjugated to nanoparticles with various core diameters. Between 401 and 475 μg of lactoferrin was added to 1 mg of PMAO-IONPs with core diameters of 14–26 nm (Table 2). The average number of lactoferrin molecules per single nanoparticle was calculated by assuming molecular weight of 90 kDa for lactoferrin and density of 5180 kg m^{-3} for iron oxide (Fe_3O_4) nanoparticles and using ICP for determination of iron concentration in each sample. Since 1 mg of IONPs contain 1×10^{14} particles for 14 nm IONPs and 2×10^{13} particles for 26 nm IONPs, and almost the same amount of lactoferrin molecules were conjugated to PMAO-IONPs regardless of their core sizes, the number of lactoferrin per particle increased as the core diameter increased from 14 nm to 26 nm (Table 2). The result of Bradford assay also indicates that 80–95% of lactoferrin added during the conjugation process was conjugated to the surface of nanoparticles.

Fig. 2 shows the TEM images of Lf-IONPs, MPS signals, and their calculated ac hysteresis loops for PMAO-IONPs and Lf-IONPs measured by our custom-built magnetic particle spectrometer (MPS).[20,29] TEM images show spherical nanoparticles with uniform size distribution for all the core diameters, which agreed with our previous report.[32] Comparing the MPS signals of nanoparticles before and after lactoferrin conjugation, PMAO-IONPs and Lf-IONPs showed similar signals. Higher signal intensities, narrower peaks, and a slight shift in the position of maximum intensities were observed with increasing core diameters of the PMAO-IONPs and Lf-IONPs. Under ac magnetic field at 26 kHz, the measured magnetic hysteresis loops differed from DC measurements by VSM (measured at room temperature for a measurement time of ~100 s). Superparamagnetic behavior and slightly open hysteresis loops were observed for the nanoparticles with core diameters of 14 nm and 16 nm under ac magnetic field, respectively. In contrast, ferromagnetic behaviors were observed for the nanoparticles with the core diameters of 20–26 nm under ac magnetic field. In MPS, the time-varying magnetization of nanoparticles under ac magnetic field induces a signal in a receiver coil. Our MPS measures the nanoparticles magnetic response, and records it as a differential susceptibility, dm/dH or $\chi_{diff}(H)$; note that an integration of the measured differential susceptibility gives the actual ac hysteresis loop. According to X-space MPI image reconstruction theory, the height and the FWHM of the measured response indicate the signal intensity and the spatial resolution of an equivalent MPI signal, respectively.[33] Comparing the MPS signals of nanoparticles before and after lactoferrin conjugation, no significant change in $\chi_{diff}(H)$ was observed for all the core diameters. This is because the MPS signal is dominated by Néel relaxation; in other words, the Brownian relaxation which is determined by the physical rotation of the nanoparticles, thus its hydrodynamic size, plays a negligible role. Higher intensity signals and smaller FWHMs were observed with increasing core diameter for both PMAO-IONPs and Lf-IONPs. These results agree with previous reports, which revealed that MPS signal strongly depends on the median core diameter of the iron oxide nanoparticles.[20,21] Although all the particles showed superparamagnetic behavior under a slowly-varying magnetic field in VSM measurements (typical measurement time ~100 s), ferromagnetic behavior with an open hysteresis loop was observed for 16–26 nm nanoparticles under the MPS ac magnetic field at a frequency of 26 kHz (measurement time ~20 μs). Furthermore, the coercivity of the integrated ac hysteresis loops increased with the core diameter and shifted the maximum intensity (peak) in MPS to higher field values in agreement with our previous results.[21] As is well known, superparamagnetic magnetite particles show zero coer-

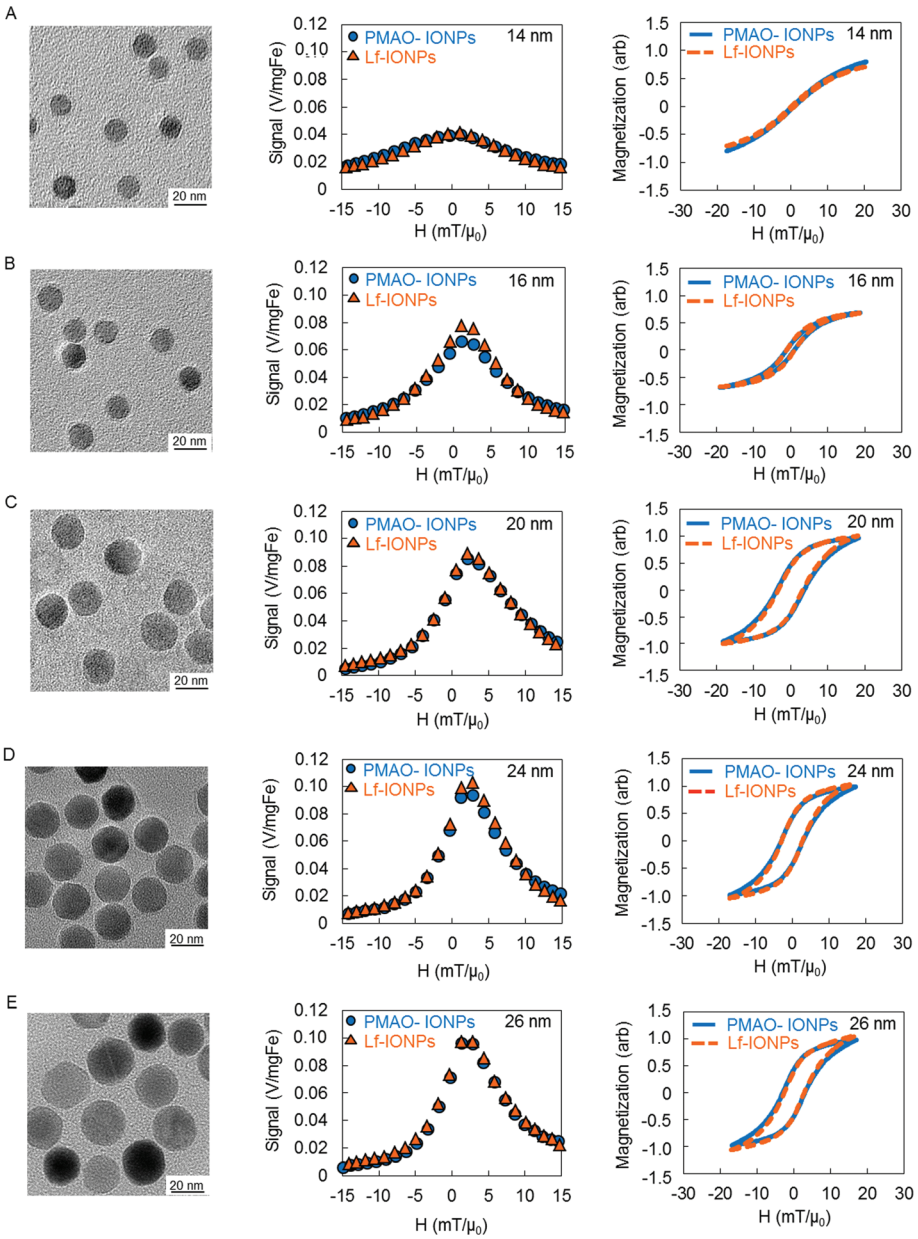

Fig. 2 TEM images, MPS signals, and integrated ac magnetization curves of PMAO-IONPs and Lf-IONPs with core diameters of (A) 14 nm (14 nm-Lf-IONPs), (B) 16 nm (16 nm-Lf-IONPs), (C) 20 nm (20 nm-Lf-IONPs), (D) 24 nm (24 nm-Lf-IONPs), and (E) 26 nm (26 nm-Lf-IONPs). The signals were divided by the amount of iron in each sample, and ac hysteresis loops were calculated by integration of the MPS signal (dm/dH). The MPS signals remained unchanged and independent of their coating compositions (PMAO or lactoferrin) for each core diameter.

civity and remanence in DC measurements, as the thermal energy is sufficient to overcome the anisotropy energy barrier and the magnetic moment of the particles fluctuates randomly within the measurement time. However under alternating magnetic field at 26 kHz, the measurement time is short enough for the magnetization to be blocked and it results in a ferromagnetic response.[1] Due to their adequate MPS signal and higher yield compared to 24 nm and 26 nm nanoparticles after phase transfer, we chose 20 nm nanoparticles for further characterization and *in vitro* study.

Fig. 3A and B show the hydrodynamic size distribution and stability (up to 4 weeks) of PMAO coated IONPs (20 nm-PMAO-IONPs) in water and lactoferrin conjugated IONPs (20 nm-Lf-IONPs) in PBS, respectively. The hydrodynamic diameters for both of 20 nm-PMAO-IONPs and 20 nm-Lf-IONPs remained unchanged for at least up to 4 weeks, due to the electrostatic repulsion of negatively charged nanoparticles and stability of lactoferrin. Our studies show that PMAO or conjugates of PMAO with other molecules usually stabilize the nanoparticles in aqueous phases due to hydrophobic inter-

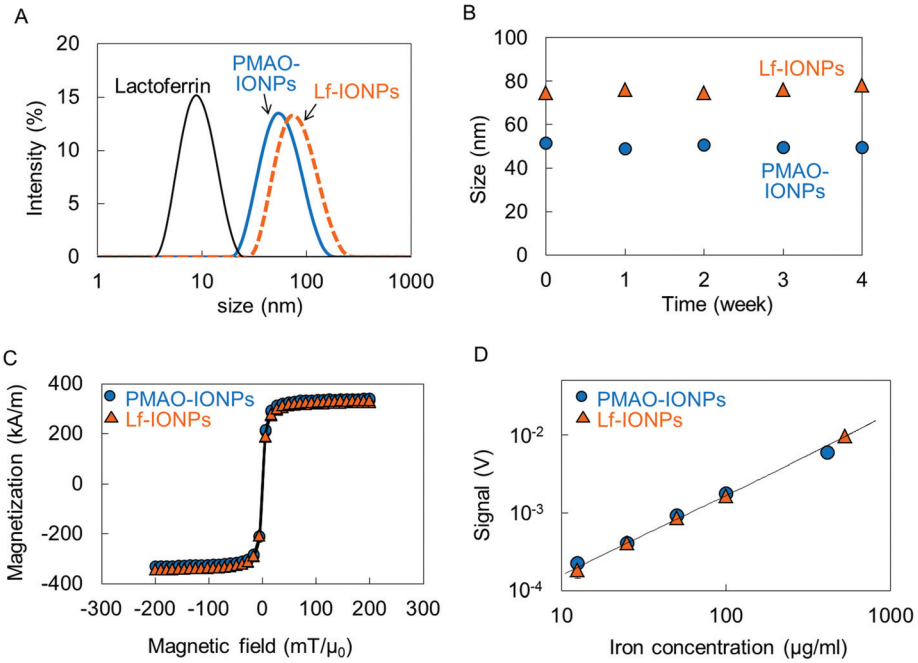

Fig. 3 (A) Hydrodynamic size distribution and (B) stability over time of PMAO-IONPs and Lf-IONPs with core diameters of 20 nm. The average hydrodynamic diameters of lactoferrin, PMAO-IONPs, and Lf-IONPs were 8 nm, 52 nm, and 75 nm, respectively. These nanoparticles were stable for up to 4 weeks. (C) DC magnetization curves and (D) MPS signal of 20 nm-PMAO-IONPs and 20 nm-Lf-IONPs as a function of iron concentration. PMAO-IONPs and Lf-IONPs exhibited identical DC magnetization curves with superparamagnetic behaviors. Lf-IONPs showed linear signal variation with increasing nanoparticles concentration.

action. For example, we have shown the long-term stability in biological buffers, cell culture media, and mice blood for the iron oxide nanoparticles coated with a PAMO-PEG (polyethylene glycol) co-polymer.[10,34,35]

Fig. 3C shows the DC magnetization curves of 20 nm-PMAO-IONPs and 20 nm-Lf-IONPs. Our VSM results showed identical magnetic behavior with superparamagnetic property for these nanoparticles. It demonstrates that lactoferrin conjugation had no influence on the DC magnetization of the nanoparticles. The saturation magnetization of 20 nm-PMAO-IONPs and 20 nm-Lf-IONPs were 71% and 70% of bulk saturation value for magnetite (92 $Am^2 kg^{-1}$),[36] respectively.

Furthermore, it is important to determine the binding affinity of lactoferrin after their conjugation to the nanoparticles. Conformational changes of proteins after conjugation to nanoparticles have been reported before.[37,38] These changes have influence on protein function, which might reduce their targeting ability. Lower binding affinity of antibody conjugated to the nanoparticles has also been reported due to the partial blocking of binding sites.[39] Therefore, we used ELISA assay to determine the binding affinity of lactoferrin after their conjugation to the nanoparticles using a polyclonal antibody specific for lactoferrin. Lactoferrin conjugated to iron oxide nanoparticles (20 nm-PMAO-IONPs) exhibited binding affinity of 32% compared to that of the same amount of free lactoferrin, which was not conjugated to the nanoparticles. It indicates conformational change or partial blocking of their binding sites after conjugation to the nanoparticles.

Fig. 3D shows the maximum intensity of the MPI signals of 20 nm-PMAO-IONPs and 20 nm-Lf-IONPs as a function of iron concentration in the biologically relevant range of 3–500 μg ml^{-1}. Both of the nanoparticles showed linear signal variations with the iron concentration in agreement with our previous reports.[21] The MPS signals were linear up to 500 μg Fe ml^{-1}, because of the increase of magnetization with the particle concentration. This linearity of the MPS signal with Fe concentration enables quantitative image interpretation using MPI.

We studied the internalization of Lf-IONPs into C6 cells by Prussian blue staining and confocal microscopy. Optical microscopy images in Fig. 4A show the Prussian blue staining of PMAO-IONPs and Lf-IONPs inside or on the surface of C6 cells after 24 h incubation with nanoparticles. More blue color regions were observed for the C6 cells incubated with Lf-IONPs compared to those incubated with PMAO-IONPs. For further confirmation of the nanoparticles internalization, Lf-IONPs were labelled by a near infrared fluorescent agent (Cy5.5), and fluorescent images were taken by confocal microscopy. Fig. 4B shows the confocal image of Cy5.5-Lf-IONPs internalized into C6 cells after 24 h incubation with nanoparticles. Taken together, it is apparent that Lf-IONPs were internalized into most of the C6 cells after 24 h incubation. Lactoferrin shows great potential as a ligand for brain tumor targeting because of the high expression of lactoferrin receptor (LRP) in glioma

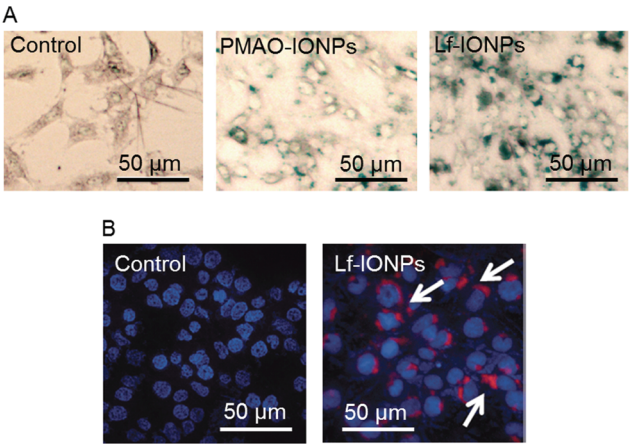

Fig. 4 (A) Prussian blue staining after 24 h incubation of C6 cells without nanoparticles (control), with PMAO-IONPs, and Lf-IONPs, showing higher uptake for Lf-IONPs as compared with PMAO-IONPs. Images were taken with inverted microscope at 20×. (B) Confocal images of C6 cells after 24 h incubation without nanoparticles (control), and with Cy5.5 labelled Lf-IONPs (white arrow). Blue regions show the DAPI stained nucleus and red spots represent the Lf-IONPs labelled by Cy5.5.

cells.[23,24] LRP-mediated endocytosis is considered to be the main mechanism of cellular uptake of lactoferrin conjugated nanoparticles.[40] Those nanoparticles taken up through endocytosis localize within endosomes which are the intracellular vesicles that fuse with lysosomes at later stages.[41]

Fig. 5 shows the MPS signals of the PMAO-IONPs and Lf-IONPs internalized into C6 cells after 2, 4, 6, 12 and 24 h incubation. Higher signal intensities were observed for internalized Lf-IONPs in comparison with internalized PMAO-IONPs at all time points while, as expected, no signal was observed for control C6 cells. Lf-IONPs internalized into C6 cells showed significant increase of MPS signal intensity after 12 h incubation, and five-fold increase in the intensity compared to PMAO-IONPs after 24 h incubation. Since MPS signal is generated only from iron oxide nanoparticles, these results suggest

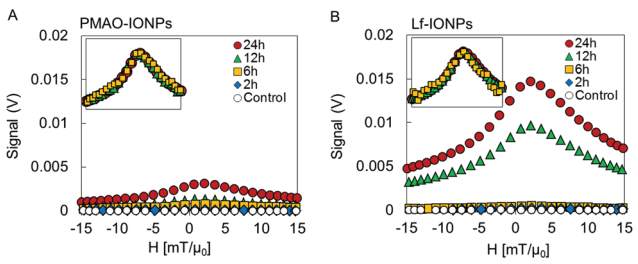

Fig. 5 MPS signals and their normalized data (inset) of C6 cells in DMEM medium (control), (A) C6 cells after incubation with PMAO-IONPs for 2, 6, 12, and 24 h, and (B) C6 cells after incubation with Lf-IONPs for 2, 6, 12, and 24 h. Higher signal intensities were observed for C6 cells incubated with Lf-IONPs compared to those with PMAO-IONPs. FWHM remained the same between incubation time of 6 to 24 h.

that significant amount of Lf-IONPs are internalized into C6 cells after 12 h incubation, and Lf-IONPs was internalized more actively compared to PMAO-IONPs. Full width at half maximum (FWHM) of internalized Lf-IONPs remained the same between incubation time of 6 to 24 h, promising a consistent spatial resolution in a real MPI scanner after nanoparticles internalization.

The concentration of Lf-IONPs internalized into C6 cells after 6 h, 12 h, and 24 h incubation was calculated to be 26, 487, 738 μg Fe ml^{-1}, respectively. These concentrations were calculated with comparing the maximum $\chi_{diff}(H)$ of internalized Lf-IONPs (Fig. 5B) and linear signal of$\chi_{diff}(H)$ against Fe concentration in solutions (Fig. 3D). We assumed that the relaxation behavior of Lf-IONPs inside the cells is the same as the Lf-IONPs in solution.

There is a broadening of the MPS signal (FWHM) and a shift in the maximum of $\chi_{diff}(H)$ to higher fields, for the Lf-IONPs after internalization. MPS performance of nanoparticles depends on particle core and hydrodynamic diameters, size distributions and their environment.[19–21] After internalization of the nanoparticles into the C6 cells, they accumulate in lysosomes and degrade in the low pH environment with the presence of chelating agents.[42] These results are consistent with our previous reports showing that FWHM of MPS signal increases and the signal peak shifts to higher field values when iron oxide nanoparticles are partially dissolved and aggregated in a lysosome-like acidic buffer.[43] Also, we have seen the same trends after internalization of the nanoparticles into the liver and spleen in mice models.[17] Since MPI spatial resolution corresponds to FWHM of the MPS signals, development of surface modification approaches to prevent degradation and aggregation of the nanoparticles would improve the spatial resolution in MPI scanners. To our knowledge, this is the first report on evaluation of *in vitro* MPI performance of iron oxide nanoparticles with a tumor targeting ability. The results presented here indicate the potential of Lf-IONPs as tracers for brain tumor imaging in animal models using MPI which is a new and safe imaging technique.

Conclusions

Lactoferrin was successfully conjugated to monodisperse iron oxide nanoparticles with the median core diameters of 14–26 nm for brain glioma targeting; the larger (>20 nm) monodisperse nanoparticles are highly optimized as efficient MPI tracers and generate higher MPI signal intensity and better spatial resolution (*i.e.* narrower FWHM) under ac magnetic field. The binding affinity of the lactoferrin conjugated nanoparticles shows their targeting ability for brain glioma diagnosis, with the MPS signal remaining unchanged after lactoferrin conjugation. Lactoferrin-conjugated nanoparticles were successfully internalized into C6 glioma cells due to the binding affinity of lactoferrin to glioma cells. *In vitro* MPS of our optimized Lf-IONPs demonstrated their potential use as tracers for brain glioma imaging using MPI.

Acknowledgements

This work was supported in part by NIH Grant No. 1RO1EB013689-01/NIBIB and NIH/NIBIB 2R42EB013520-02A1. Part of this work was conducted at the University of Washington NanoTech User Facility, a member of the NSF National Nanotechnology Infrastructure Network (NNIN). AT was also supported (2012–14) by the Japan Society for the Promotion of Science Postdoctoral Fellowship for Research Abroad.

References

1 K. M. Krishnan, *IEEE Trans. Magn.*, 2010, **46**, 2523–2558.
2 M. Arruebo, R. Fernandez-Pacheco, M. R. Ibarra and J. Santamaria, *Nanotoday*, 2007, **2**, 22–32.
3 T. K. Jain, J. M. Richey Strand, D. L. Leslie-Pelecky, C. A. Flask and V. Labhasetwar, *Biomaterials*, 2008, **29**, 4012–4021.
4 D. Kami, S. Takeda, Y. Itakura, S. Gojo, M. Watanabe and M. Toyoda, *Int. J. Mol. Sci.*, 2011, **12**, 3705–3722.
5 R. D. Jayant, V. S. R. Atluri, M. Agudelo, V. Sagar, A. Kaushik and M. Nair, *Int. J. Nanomed.*, 2015, **10**, 1077–1093.
6 B. Chertok, B. A. Moffat, A. E. David, F. Yu, C. Bergemann, B. D. Ross and V. C. Yang, *Biomaterials*, 2008, **29**, 487–496.
7 L. Yang, X. Ren, F. Tang and L. Zhang, *Biosens. Bioelectron.*, 2009, **25**, 889–895.
8 D. Wang, J. He, N. Rosenzweig and Z. Rosenzweig, *Nano Lett.*, 2004, **4**, 409–413.
9 A. Tomitaka, T. Yamada and Y. Takemura, *J. Nanomater.*, 2012, **5**, 480626.
10 A. P. Khandhar, R. M. Ferguson, J. A. Simon and K. M. Krishnan, *J. Biomed. Mater. Res.*, 2011, **100A**, 728–737.
11 B. Gleich and J. Weizenecker, *Nature*, 2005, **435**, 1214–1217.
12 J. Weizenecker, B. Gleich, J. Rahmer, H. Dahnke and J. Borgert, *Phys. Med. Biol.*, 2009, **54**, L1–10.
13 M. R. Ferguson, A. P. Khandhar AP, S. J. Kemp, H. Arami, E. U. Saritas, L. R. Croft, J. Konkle, P. W. Goodwill, A. Halkola, J. Rahmer, J. Borgert, S. M. Conolly and K. M. Krishnan, *IEEE Trans. Med. Imaging*, 2015, **34**(5), 1077–1084.
14 L. M. Bauer, S. F. Situ, M. A. Griswold and A. C. S. Samia, *J. Phys. Chem. Lett.*, 2015, **6**, 2509–2517.
15 E. M. Saritas, P. W. Goodwill, L. R. Croft, J. J. Konkle, K. Lu, B. Zheng and S. M. Conolly, *J. Magn. Res.*, 2013, **229**, 116–126.
16 T. H. Shin, Y. Choi, S. Kim and J. Cheon, *Chem. Soc. Rev.*, 2015, **44**, 4501–4516.
17 H. Arami, A. P. Khandhar, A. Tomitaka, E. Yu, P. W. Goodwill, S. M. Conolly and K. M. Krishnan, *Biomaterials*, 2015, **52**, 251–261.
18 M. H. Pablico-Lansigan, S. F. Situ and A. C. S. Samia, *Nanoscale*, 2013, **5**, 4040–4055.
19 R. M. Ferguson, A. P. Khandhar and K. M. Krishnan, *J. Appl. Phys.*, 2012, **111**, 07B318.
20 R. M. Ferguson, K. R. Minard, A. P. Khandhar and K. M. Krishnan KM, *Med. Phys.*, 2011, **38**, 1619–1626.
21 H. Arami, R. M. Ferguson, A. P. Khandhar and K. M. Krishnan, *Med. Phys.*, 2013, **40**, 071904.
22 L. Adlerova, A. Bartoskova and M. Faldyna, *Vet. Med.*, 2008, **53**, 457–468.
23 H. Xie, Y. Zhu, W. Jiang, Q. Zhou, H. Yang, N. Gu, Y. Zhang, H. Xu, H. Xu and X. Yang, *Biomaterials*, 2011, **32**, 495–502.
24 Z. Pang, L. Feng, R. Hua, J. Chen, H. Gao, S. Pan, X. Jiang and P. Zhang, *Mol. Pharm.*, 2010, **7**, 1995–2005.
25 R. Huang, W. Ke, L. Han, Y. Liu, K. Shao, L. Ye, J. Lou, C. Jiang and Y. Pei, *J. Cereb. Blood Flow Metab.*, 2009, **29**, 1914–1923.
26 K. Hu, J. Li, Y. Shen, W. Lu, X. Gao, Q. Zhang and X. Jiang, *J. Controlled Release*, 2009, **134**, 55–61.
27 S. Kalele, R. Narain and K. M. Krishnan, *J. Magn. Magn. Mater.*, 2009, **321**, 1377–1380.
28 R. Narain, M. Gonzales, A. S. Hoffman, P. S. Stayton and K. M. Krishnan, *Langmuir*, 2007, **23**, 6299–6304.
29 R. M. Ferguson, A. Khandhar, H. Arami, L. Hua, O. Hovorka and K. M. Krishnan, *Biomed. Eng.*, 2013, **58**, 1–15.
30 F. Ludwig, H. Remmer, C. Kuhlmann, T. Wawrzik, H. Arami, R. M. Ferguson and K. M. Krishnan, *J. Magn. Magn. Mater.*, 2014, **360**, 169–173.
31 M. Moros, B. Pelaz, P. López-Larrubia, M. L. Garía-Martin, V. Grazú and J. M. Fuente, *Nanoscale*, 2010, **2**, 1746–1755.
32 R. Hufschmid, H. Arami, R. M. Ferguson, M. Gonzales, E. Teeman, L. N. Brush, N. D. Browning and K. M. Krishnan, *Nanoscale*, 2015, **7**, 11142–11154.
33 P. Goodwill, E. U. Saritas, L. R. Croft, T. N. Kim, K. M. Krishnan, D. V. Schaffer and S. M. Conolly, *Adv. Mater.*, 2012, **24**, 3870–3877.
34 W. Yu, E. Chang, C. M. Sayes, R. Drezek and V. L. Colvin, *Nanotechnology*, 2006, **17**, 4483–4487.
35 A. P. Khandhar, R. M. Ferguson, H. Arami and K. M. Krishnan, *Biomaterials*, 2013, **34**, 3837–3845.
36 T. Sato, T. Iijima, M. Seki and N. Inagaki, *J. Magn. Magn. Mater.*, 1987, **65**, 252–256.
37 I. Lynch and K. A. Dawson, *Nanotoday*, 2008, **3**, 41–47.
38 M. Mahmoudi, M. A. Shokrgozar, S. Sardari, M. K. Moghadam, H. Vali, S. Laurent and P. Stroeve, *Nanoscale*, 2011, **3**, 1127–1138.
39 S. Wang, N. Mamedova, N. A. Kotov, W. Chen and J. Studer, *Nano Lett.*, 2002, **2**, 817–822.
40 Z. Su, L. Xing, Y. Chen, Y. Xu, F. Yang, C. Zhang, Q. Ping and Y. Xiao, *Mol. Pharm.*, 2014, **11**, 1823–1834.
41 T. G. Iversen, T. Skotland and K. Sandvig, *Nano Today*, 2011, **6**, 176–185.
42 A. Tomitaka, J. Jo, I. Aoki and Y. Tabata, *Inflammtion Regener.*, 2014, **34**, 45–55.
43 H. Arami and K. M. Krishnan, *J. Appl. Phys.*, 2014, **115**, 17B306.

